PHYSICAL REVIEW E **87**, 011002(R) (2013)

Effective hydrodynamic boundary conditions for microtextured surfaces

Anne Mongruel,[1] Thibault Chastel,[1] Evgeny S. Asmolov,[2,3,4] and Olga I. Vinogradova[2,5,6]

[1]*Physique et Mécanique des Milieux Hétérogènes (PMMH), UMR 7636 CNRS; ESPCI ParisTech; Université Pierre et Marie Curie (UPMC); Université Paris Diderot (Paris 7) 10 rue Vauquelin, 75231 Paris cedex 05, France*

[2]*A.N. Frumkin Institute of Physical Chemistry and Electrochemistry, Russian Academy of Sciences, 31 Leninsky Prospect, 119991 Moscow, Russia*

[3]*Central Aero-Hydrodynamics Institute, 1 Zhukovsky Street, Zhukovsky, Moscow Region 140180, Russia*

[4]*Institute of Mechanics, M. V. Lomonosov Moscow State University, 119992 Moscow, Russia*

[5]*Department of Physics, M. V. Lomonosov Moscow State University, 119991 Moscow, Russia*

[6]*DWI, RWTH Aachen, Forckenbeckstrasse 50, 52056 Aachen, Germany*

(Received 26 March 2012; published 8 January 2013)

Understanding the influence of topographic heterogeneities on liquid flows has become an important issue with the development of microfluidic systems, and more generally for the manipulation of liquids at the small scale. Most studies of the boundary flow past such surfaces have concerned poorly wetting liquids for which the topography acts to generate superhydrophobic slip. Here we focus on topographically patterned but chemically homogeneous surfaces, and measure a drag force on a sphere approaching a plane decorated with lyophilic microscopic grooves. A significant decrease in the force compared with predicted even for a superhydrophobic surface is observed. To quantify the force we use the effective no-slip boundary condition, which is applied at the imaginary smooth homogeneous isotropic surface located at an intermediate position between the top and bottom of grooves. We relate its location to a surface topology by a simple, but accurate analytical formula. Since grooves represent the most anisotropic surface, our conclusions are valid for any texture, and suggest rules for the rational design of topographically patterned surfaces to generate desired drag.

DOI: 10.1103/PhysRevE.87.011002 PACS number(s): 47.90.+a, 68.08.−p, 68.35.Ct

I. INTRODUCTION

The advent of microfluidics has motivated the growing interest in understanding and modeling of flows at small scales or in tiny channels. In recent years it has become clear that the no-slip boundary condition at a solid-liquid interface is valid only for smooth hydrophilic surfaces [1–4], and for many other systems it does not apply when the size of a system is reduced. Thus the hydrophobicity of smooth surfaces could induce a partial slippage, $v_s = b\partial v/\partial z$, where v_s is the velocity at the wall, b is the slip length, and the axis z is normal to the surface [5]. This concept is now well supported by nanorheology measurements [1,2,4].

However, only very few solids are molecularly smooth. Most of them are rough, often at a micrometer scale. This roughness may be induced by some processes of fabrication or coating, but microtextures are also found on the surfaces of most plants and animals. In particular, many solids are naturally striated by grooves, which can also be prepared for specific microfluidic purposes, such as passive chaotic mixing [6,7]. Most studies of flow past rough surfaces have concerned poorly wetting liquids for which the topography acts to favor the formation of trapped gas bubbles (Cassie state), and to generate superhydrophobic slippage [8,9]. For rough wettable surfaces the situation is unclear, and opposite conclusions have been made: one is that roughness generates extremely large slip [10], and the other is that it decreases the degree of slippage [11]. Recent data (supported by simulations [12]) suggest that the description of flow near rough surfaces has to be corrected, but rather for a separation, not a slip [13,14]. Another suggestion is to combine these two models [15].

In this Rapid Communication we describe how the boundary conditions can be modified by the surface texture. We focus on the case of special interest where this model surface is decorated by rectangular microgrooves, i.e., on the situation of the largest possible anisotropy of the flow. We analyze the hydrodynamic interaction between a smooth sphere and a grooved plane, as sketched in Fig. 1, and the texture parameters are systematically varied at the micrometer level, in order to investigate their influence on a drag force. Our results do not support some previous experimental conclusions on a large slip for similar systems. Instead, we unambiguously prove the concept of an effective no-slip plane shifted down from the top of roughness. In this study, experimentally found values of this shift were quantified theoretically and related analytically to controlled parameters of topographic patterns.

II. EXPERIMENT

We use a specially designed homemade setup [16–18] to measure on a microscale the displacement of a sphere towards the corrugated wall at constant gravity force. The steel sphere of density $\rho_p = 7.8 \times 10^3$ kg m^{-3} and radii ranging from 3.5 to 6.35 mm is embedded in a liquid contained in a cylindrical glass vessel with a 50 mm diameter and a 40 mm height. As a liquid we have chosen high molecular weight PDMS (silicone) oil (47V100000 Rhodorsyl oil, from Rhone-Poulenc), with dynamic viscosity $\mu = 97.8$ Pa s at 25 °C, which is Newtonian for shear rates up to 100 s^{-1}. Such shear rates are never reached in our experiment.

The microstructured surfaces were created by common soft lithography, in a three step process, transferring geometric shapes from a mask: first to a silicon wafer coated with a (SU8) photoresist, second to a replica molding obtained by soft imprint of a thermoreticulable PDMS, and finally to a replica of

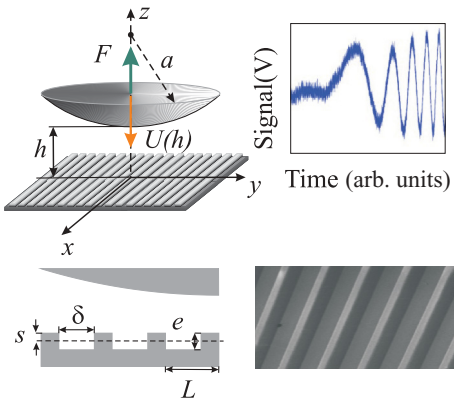

FIG. 1. (Color online) Sketch of a sphere approaching a model grooved surface (left) with the example of a typical experimental signal and a scanning electron micrograph (taken under an angle) of the surface obtained by a soft lithography (right).

the PDMS mold by soft imprint of a thiolene based resin (NOA 81, Norland optical adhesives) on glass microscope slides (to be fixed at the bottom of the vessel). This resin was chosen for its resistance to compression and to solvent swelling, and for its good adhesion to glass [19]. The final structures are checked by scanning electron microscopy (see Fig. 1). The textures are characterized by spacing δ, height e, and period L. The liquid fraction $\phi = \delta/L$ can be precisely measured since it is the ratio of the upper surface of the crenellations over the total surface of the sample. It varies largely with the patterns (from 0.1 to 0.9), and e/L varies from 0.168 to 0.45, as displayed in Table I. Contact angles against PDMS for all textures were found to be below 30°, so that surfaces can be considered as lyophilic. Therefore, we expect PDMS to invade the surface texture (Wenzel state).

We measure the distance h, which is defined from the top of the textures (contact) by using an interferometric technique [16–18] with accuracy 0.2 μm. The velocity $U(h)$ of the sphere is found by multiplying the velocity of interference fringes displacement by a factor of $\lambda/2n$, where $\lambda = 632.8$ nm is the wavelength of the He-Ne laser, and $n = 1.404$ is the refraction index of PDMS. After optoelectronic conversion and amplification, the signal is recorded with a high frequency electronic oscilloscope (DPO4032 from Tektronics). A deceleration of the sphere (Fig. 1) is reflected in the increase of the period of the signal, until contact occurs, and its position is defined from the recorded signal, at the time when the period of the signal becomes very large indicating a vanishing velocity. Note that the signal-to-noise ratio deteriorates at vanishing frequency, because the low frequency limit of the oscilloscope is reached. The measured frequency is averaged over seven to eight periods, except just before the contact, where no averaging is applied in order to capture the rapid velocity variations occurring in that region.

TABLE I. Parameters of the textured samples and the shift of effective hydrodynamic wall, s.

No.	L (μm)	δ (μm)	ϕ	e (μm)	s, experiment (μm)	s, theory [Eqs. (4), (6), and (7)] (μm)
1	100	50	1/2	45	5 ± 0.1	5.5
2	150	50	1/3	45	4.2 ± 0.3	3.5
3	150	100	2/3	45	13 ± 2	11.8
4	200	100	1/2	76	13 ± 3	10.4
5	200	100	1/2	45	9 ± 1.5	8.3
6	250	25	1/10	42	0.5 ± 0.1	0.6
7	250	225	9/10	42	28.5 ± 0.5	23.5

III. RESULTS AND DISCUSSION

Figure 2 shows the drag F (equal to the gravity force) scaled by the Stokes force $F_{St} = 6\pi\mu a U(h)$, i.e., $U(\infty)/U(h)$. The solid line is a theoretical force (Taylor's equation) predicted for a case of smooth wall and no slippage at the surface:

$$F_T/F_{St} = a/h. \quad (1)$$

Also included are the experimental data for samples with similar e, but different ϕ and L, which show deviations from the behavior predicted by Eq. (1). Close to the wall, for $a/h > 50$, the drag is always significantly less than the force near a smooth wall, and this reduction increases with ϕ. To examine these deviations we evaluate a correction to the drag force,

$$f^*(h) = F(h)/F_T(h). \quad (2)$$

Note that in general, the case for a rough surface f^* should also depend on the radius of the sphere [12]. However, with our configuration geometry experimental data do not vary with a. This is well illustrated in Fig. 3(a), where the experimental values of f^* obtained with sample No. 7 at different a and plotted as a function of h/L collapse into a single curve, which tends to unity at large distances and decreases significantly when h becomes of the order of L and smaller. Since at short separations we observe $f^* \to 0$, one can conclude that slippage (which would lead to $f^* \to 1/4$ [20]) obviously does not mimic roughness when h is small, by overestimating the drag force. The same remark concerns effective superhydrophobic slippage where $f^* \to 2(4-3\phi)/(8+9\phi-9\phi^2)$ [21] and is equal to $\simeq 0.3$ for this particular sample.

Therefore, our experimental results are now compared with theoretical calculations made for an effective smooth plane shifted down from the top of the corrugations, i.e., by assuming

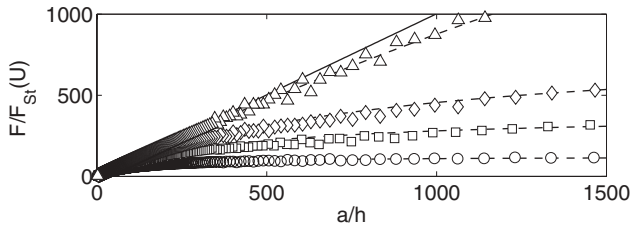

FIG. 2. Normalized drag (symbols) as a function of a/h. From top to bottom the data sets for samples Nos. 6, 2, 5, and 7 (see Table I). Solid line shows the theoretical prediction for a smooth lyophilic wall, Eq. (1), defined at the top of grooves. The dashed curves from top to bottom are calculations of the force expected for a smooth lyophilic wall shifted from the textured wall to a distance $s = 0.5$, 4.2, 9, and 28.5 μm.

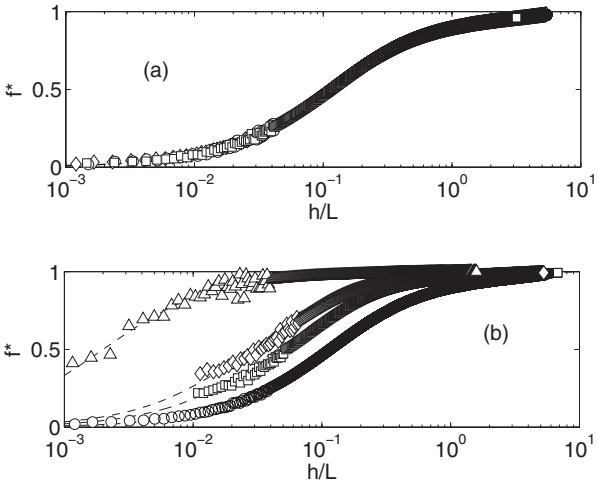

FIG. 3. Measured correction to drag (symbols) (a) for spheres of different radii ($a = 3.5$, 5.75, and 6.35 mm) interacting with sample No. 7. Dashed line shows the calculated correction, using $s = 28.5$ μm in Eq. (3), (b) for striped walls having nearly same e, but different ϕ and L; from left to right: samples Nos. 6, 2, 5, and 7. Dashed lines: model, Eq. (3), with (a) $s = 28.5$ μm and (b) from left to right: $s = 0.5$, 4.2, 9, and 28.5 μm.

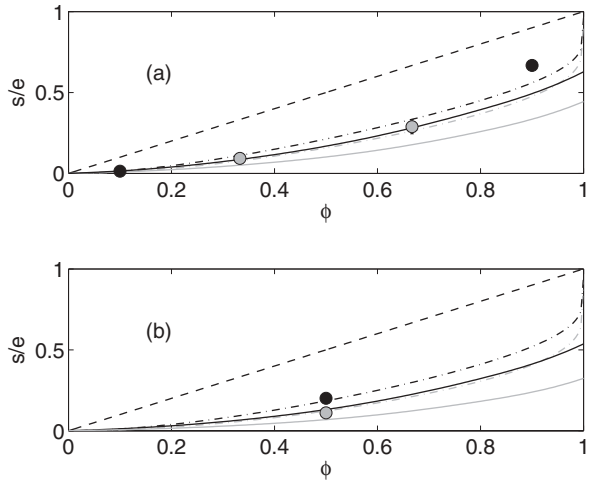

FIG. 4. Experimental values of s/e (symbols) as a function of ϕ for grooves with similar heights, but different ϕ and L. Lines show theoretical predictions, Eq. (4), where $b_{\rm eff}^{\parallel}$and $b_{\rm eff}^{\perp}$ are calculated by using the analysis of [23] (solid lines), Eqs. (6) and (7) (dash-dotted lines), and Eq. (5) (dashed lines): (a) samples Nos. 6 and 7 (black), samples Nos. 2 and 3, (gray); (b) sample No. 5 (black) and sample No. 1 (gray).

$F(h) = F_T(h + s)$, where s is the value of *constant*, i.e., independent on h, shift. This implies that

$$f^*(h) = \frac{F_T(h+s)}{F_T(h)} = \frac{h}{h+s}. \tag{3}$$

Figure 3(a) includes a calculation (dashed curve) in which an adjustable parameter, a shift of $s = 28.5$ μm, is incorporated into the Taylor equation. The fit is very good for all h, suggesting the validity of the model. Figure 3(b) shows another series of experiments made with the fixed radius of the sphere, but different parameters of the texture. If similar fits are made to a variety of experiments it is found that the shift of an equivalent plane required to fit each run increases from 0.5 μm for sample No. 2 to 28.5 μm for sample No. 7. In Table I we present the experimental values of s for different samples, and curves calculated with Eq. (3) are included in Figs. 2 and 3. The fit is excellent at all separations except as very small, $h/L \leqslant 0.01$. Thus our experiment shows that an effective (scalar) shift s is a unique physical parameter that fully quantifies drag reduction at a highly anisotropic corrugated surface. This striking result indicates that in our experiment pressure remains isotropic despite an anisotropy of the flow.

Now we try to relate s to parameters of textured surfaces. As proven in [17,21], for a large gap $h \gg L$ the shift of the equivalent no-slip plane from the real surface is equal to the average of the eigenvalues of the effective slip-length tensor (at the slip plane defined at the top of asperities)

$$s \simeq \frac{b_{\rm eff}^{\parallel} + b_{\rm eff}^{\perp}}{2}. \tag{4}$$

Therefore, the problem of calculating s reduces to computing the two far-field eigenvalues $b_{\rm eff}^{\parallel}$ and $b_{\rm eff}^{\perp}$, which attain the maximal and minimal directional slip lengths, respectively. In the limit $e \ll L \ll h$, the theory [22] predicts that the effective no-slip surface for arbitrary smooth periodic surfaces is at the average height:

$$b_{\rm eff}^{\parallel,\perp} \simeq \phi e, \tag{5}$$

so that s/e is controlled mainly by ϕ. To examine the significance of ϕ more closely, the experimental s normalized by e are reproduced in Fig. 4. The measured data show much smaller s/e than the theoretical prediction of model (5) shown by a dashed line. A possible explanation for this discrepancy is that the height of asperities in our experiments was not small enough, $0.168 \leqslant e/L \leqslant 0.45$. We also compared our data with another calculation (solid curves) for hydrophilic grooves with finite e/L based on numerical results [23] for eigenvalues of the slip-length tensor. Even at moderate e/L theoretical predictions for s [23] are much smaller than measured values.

An alternative model can be obtained if we use the analytic solutions for alternating slip and no-slip stripes [24]:

$$b_{\rm eff}^{||} \simeq \frac{L}{\pi} \frac{\ln\left[\sec\left(\frac{\pi\phi}{2}\right)\right]}{1 + \frac{L}{\pi e}\ln\left[\sec\left(\frac{\pi\phi}{2}\right) + \tan\left(\frac{\pi\phi}{2}\right)\right]}, \tag{6}$$

$$b_{\rm eff}^{\perp} \simeq \frac{L}{2\pi} \frac{\ln\left[\sec\left(\frac{\pi\phi}{2}\right)\right]}{1 + \frac{L}{2\pi e}\ln\left[\sec\left(\frac{\pi\phi}{2}\right) + \tan\left(\frac{\pi\phi}{2}\right)\right]}, \tag{7}$$

where we naturally assumed that the local partial slip is equal to the height of grooves. Figure 4 shows that Eq. (4) together with Eqs. (6) and (7) (dashed curves) give almost quantitative agreement with experimental data. (We also include theoretical values of s in Table I to allow a direct comparison with experimental results.) Therefore, by using the equivalence of a flow past rough and heterogeneous surfaces at large scale, we were able to quantify a drag reduction at the smaller scale, of the order of the size of roughness elements. Note, however, that our results do not apply to a very thin gap situation $h \ll L$, where s scales with the channel width [25], which is again consistent with our experiment.

IV. CONCLUDING REMARKS

We have studied a drag force on a sphere approaching a corrugated plane. Our experiment shows quantitatively that in this situation the effective no-slip boundary condition, which is applied at the imaginary smooth homogeneous isotropic surface located at an intermediate position between the top and bottom of grooves, fully mimics the actual one along the true corrugated interface, except as for a very thin gap. The location of this effective isotropic plane depends on the parameters of the texture, and can be found by using simple formulas for effective slip lengths in the limit of a thick channel. Since for grooves anisotropy is maximized, the same conclusion would be valid for other types of anisotropic (e.g., sinusoidal, trapezoidal, and more) and/or isotropic (e.g., pillars, etc.) textures, but of course, Eqs. (6) and (7) should be replaced by analytical or numerical solutions for a corresponding texture, as will be described in subsequent papers. We have also demonstrated that topographically patterned (Wenzel) surfaces could reduce a drag force more efficiently compared to expected even for slipping superhydrophobic (Cassie) textures with trapped gas. Therefore, our results suggested rules and a general strategy for the rational design of topographically patterned surfaces to generate desired low drag.

[1] O. I. Vinogradova and G. E. Yakubov, Langmuir **19**, 1227 (2003).
[2] C. Cottin-Bizonne, B. Cross, A. Steinberger, and E. Charlaix, Phys. Rev. Lett. **94**, 056102 (2005).
[3] L. Joly, C. Ybert, and L. Bocquet, Phys. Rev. Lett. **96**, 046101 (2006).
[4] O. I. Vinogradova, K. Koynov, A. Best, and F. Feuillebois, Phys. Rev. Lett. **102**, 118302 (2009).
[5] O. I. Vinogradova, Int. J. Min. Process. **56**, 31 (1999).
[6] A. D. Stroock, S. K. W. Dertinger, A. Ajdari, I. Mezić, H. A. Stone, and G. M. Whitesides, Science **295**, 647 (2002).
[7] F. Feuillebois, M. Z. Bazant, and O. I. Vinogradova, Phys. Rev. E **82**, 055301(R) (2010).
[8] J. P. Rothstein, Annu. Rev. Fluid Mech. **42**, 89 (2010).
[9] O. I. Vinogradova and A. V. Belyaev, J. Phys.: Condens. Matter **23**, 184104 (2011).
[10] E. Bonaccurso, H.-J. Butt, and V. S. J. Craig, Phys. Rev. Lett. **90**, 144501 (2003).
[11] Y. Zhu and S. Granick, Phys. Rev. Lett. **88**, 106102 (2002).
[12] C. Kunert, J. Harting, and O. I. Vinogradova, Phys. Rev. Lett. **105**, 016001 (2010).
[13] O. I. Vinogradova and G. E. Yakubov, Phys. Rev. E **73**, 045302(R) (2006).
[14] A. Steinberger, C. Cottin-Bizonne, P. Kleimann, and E. Charlaix, Nature Mater. **6**, 665 (2007).
[15] S. Guriyanova, B. Semin, T. S. Rodrigues, H. J. Butt, and E. Bonaccurso, Microfluid. Nanofluid. **8**, 653 (2010).
[16] N. Lecoq, F. Feuillebois, N. Anthore, R. Anthore, F. Bostel, and C. Petipas, Phys. Fluids **5**, 3 (1993).
[17] N. Lecoq, R. Anthore, B. Cichocki, P. Szymczak, and F. Feuillebois, J. Fluid Mech. **513**, 247 (2004).
[18] A. Mongruel, C. Lamriben, S. Yahiaoui, and F. Feuillebois, J. Fluid Mech. **661**, 229 (2010).
[19] D. Bartolo, G. Degre, P. Nghe, and V. Struder, Lab. Chip **8**, 274 (2008).
[20] O. I. Vinogradova, Langmuir **11**, 2213 (1995).
[21] E. S. Asmolov, A. V. Belyaev, and O. I. Vinogradova, Phys. Rev. E **84**, 026330 (2011).
[22] K. Kamrin, M. Z. Bazant, and H. A. Stone, J. Fluid Mech. **658**, 409 (2010).
[23] C. Y. Wang, Phys. Fluids **15**, 1114 (2003).
[24] A. V. Belyaev and O. I. Vinogradova, J. Fluid Mech. **652**, 489 (2010).
[25] See Supplemental Material at http://link.aps.org/supplemental/10.1103/PhysRevE.87.011002 for details of the theoretical solution for a thin channel situation.